Redox Free Energies from Vertical Energy Gaps: Ab Initio Molecular Dynamics Implementation

J. Blumberger[1] and M. Sprik[2]

[1] Center for Molecular Modeling and Department of Chemistry, University of Pennsylvania, 231 S. 34th Street Philadelphia, PA 19104-6323
[2] Department of Chemistry, University of Cambridge, Cambridge CB2 1EW, United Kingdom

Michiel Sprik

J. Blumberger and M. Sprik: *Redox Free Energies from Vertical Energy Gaps: Ab Initio Molecular Dynamics Implementation*, Lect. Notes Phys. **704**, 481–506 (2006)
DOI 10.1007/3-540-35284-8_18

1 Introduction

The development of methods for the exploration of reaction paths in condensed molecular systems (solutions and biopolymers) and the computation of the corresponding reaction free energies and kinetic parameters remains at the center of research in computational chemistry. Much has happened in recent years. It is the subject of a good number of the chapters in this book, which give an up to date overview of the enormous progress that has been made. We mention the development of the transition path sampling method by the group of Chandler at Berkeley (see the chapters by Dellago, Bolhuis and Geissler, where also the references to the original literature can be found). An alternative approach with a somewhat different purpose and scope is the metadynamics method developed by the Parrinello group (see the chapter by Laio and Parrinello). Transition path sampling and metadynamics studies to date have focused mostly on dynamical processes which never leave the adiabatic ground state potential energy surface (PES). However barriers for chemical reactions often coincide with an avoided crossing, or, alternatively, can be seen as the result of the coupling between two intersecting diabatic surfaces (see Fig. 1). The diabatic perspective offers certain advantages. This applies in particular to activation energies with a strong solvent contribution. An instructive example of such a reaction is electron transfer (ET). For outer sphere transfer the barrier is almost 100 percent due to rearrangement of the solvent polarization. This observation is a key idea in the Marcus theory of electron transfer [1–4]. In the original formulation of the theory [1] the polarization was described by the linear response of a dielectric continuum. How to quantify solvent polarization by a microscopic order parameter? Polarization is a highly collective quantity with a configurational component (the orientation of molecules) and electronic component (induced polarization).

While it should be possible to find a ground state observable incorporating all relevant aspects of the solvent response to ET, the diabatic picture at the core of Marcus theory suggests that the vertical energy gap between the two

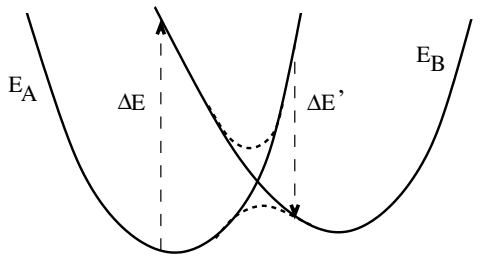

Fig. 1. Two intersecting diabatic potential energy surfaces E_{A} and E_{B} (*solid curves*). The *dashed curves* are the corresponding adiabatic surfaces. The *dashed arrows* indicate two examples of the diabatic vertical energy gap defined in (3), the gap on the left (ΔE) is positive and the one on the right ($\Delta E'$) negative

diabatic surfaces is a more suitable quantity for this purpose (see e.g. [2]). The first to use this idea in a simulation of ET reactions was Warshel [5]. A key step in his approach is the observation that the energy gap is a particularly convenient reaction coordinate for the application of free energy perturbation methods [5–11]. This enabled Warshel and coworkers to calculate not only the reaction and activation free energy from their molecular dynamics (MD) trajectories but also the reorganization free energy of Marcus theory (see below). The latter quantity, usually written as λ, is the free energy cost of deforming an equilibrium atomic configuration in the reactant state to an equilibrium configuration of the product state while staying on the diabatic PES of the reactant (so without making an electronic transition). Reorganization free energy is therefore a new quantity unique to the diabatic (two surface) picture. As the many successful applications of Marcus theory illustrate, it is a most powerful concept for the analysis and understanding of chemical reactions.

Marcus theory has inspired a rich production of simulation studies aiming to validate its assumptions or focusing on applications to specific model systems. References [6,7] and [12–27] are a selection of the many papers that have appeared since Warshel's pioneering 82 paper [5]. These studies are based on classical and semi-classical models. In a series of recent *ab initio* MD studies of redox half reactions involving transition metal coordination complexes [28–33] and organic molecules [34–36] we have attempted to implement similar methods in a density functional theory based MD (Car-Parrinello) [37] framework. A number of technical difficulties had (and some remain) to be resolved. The aim of this chapter is to discuss some of the background which our approach shares with earlier work.

2 Simulation of Electron Transfer

2.1 The Diabatic Energy Gap as Reaction Coordinate

For non-adiabatic ET treated in a semi-classical MD approximation the diabatic energy gap is the ideal reaction coordinate [5]. The electronic system in this approach is modeled by a two level system defined by a 2×2 Hamiltonian matrix

$$\mathbf{H} = \begin{pmatrix} E_{\mathrm{A}}\left(\mathbf{R}^N\right) & \gamma\left(\mathbf{R}^N\right) \\ \gamma\left(\mathbf{R}^N\right) & E_{\mathrm{B}}\left(\mathbf{R}^N\right) \end{pmatrix} \tag{1}$$

The two diagonal elements represent the diabatic PES of reactant A and product B where $\mathbf{R}^N$ are the atomic positions of (in principle) all N atoms in the system. For example in case of a charge separation reaction

$$\mathrm{D} + \mathrm{A} \rightarrow \mathrm{D}^+ + \mathrm{A}^- \tag{2}$$

the reactant state A corresponds to the donor-acceptor pair $\mathrm{D} + \mathrm{A}$ before the transfer and B to the product $\mathrm{D}^+ + \mathrm{A}^-$ after the transfer. The diabatic states

are coupled by the off-diagonal matrix element γ. This quantity depends on the overlap between the electron wavefunctions in reactant and product state and is often modelled by an exponent of the distance r_{DA} between donor and acceptor, $\gamma = \gamma_0 \exp(-\alpha r_{\mathrm{DA}})$, where α is a positive parameter with the dimension of inverse length. The vertical diabatic energy gap of the two level system of (1) is simply the difference of the diagonal matrix elements.

$$\Delta E(\mathbf{R}^N) = E_{\mathrm{B}}(\mathbf{R}^N) - E_{\mathrm{A}}(\mathbf{R}^N) \tag{3}$$

If the off-diagonal matrix element γ is small (weak coupling), for example because the distance between donor and acceptor in reaction (2) is large, the (absolute) diabatic energy gap ΔE of (3) can be identified with the adiabatic vertical excitation energy

$$\Delta E_{1\leftarrow 0}\left(\mathbf{R}^N\right) = \left[\left(E_{\mathrm{A}} - E_{\mathrm{B}}\right)^2 + 4\gamma^2\right]^{1/2} \tag{4}$$

where the index 0 denotes the ground state and 1 the (only) excited state and we have suppressed the dependence on $\mathbf{R}^N$ of the quantities on the rhs. Note, however, that ΔE of (3) can be both positive and negative, changing sign at the surface crossing. This is where, in the weak coupling limit, the radiationless transition between state A and B takes place. The vertical diabatic energy gap can therefore be used as a reaction coordinate assigning each atom configuration $\mathbf{R}^N$ either to reactant or product. Using first order time dependent perturbation theory arguments, Marcus separated the ET rate k_{ET} in a quantum transition probability proportional to the squared coupling parameter γ^2 and the Boltzmann exponent of the free energy G at the surface crossing

$$k_{\mathrm{ET}} = \kappa\gamma^2 \exp\left[-\Delta G\left(\Delta E = 0\right)/k_{\mathrm{B}}T\right] \tag{5}$$

The non-adiabatic "transition state" is unambiguously identified by the zero gap ($\Delta E = 0$). Equation (5), including the expression for the prefactor κ, can be derived using the Golden rule. The derivation is far from straightforward, requiring careful consideration of the classical limit of the atomic system (see for example [38]). An easier route is to start from a classical atomic system using a Landau Zener approach [39].

The factorization of the ET rate achieved in (5) allows us to compute the activation free energy $\Delta G\left(\Delta E = 0\right)$ treating the atoms as classical particles and make separate assumptions for the estimation of γ (or even not worry about it at all). This is the justification of the many classical force field model based simulations of non-adiabatic ET, which at first might seem somewhat of a contradiction. The vertical energy gap in the fully classical point charge model can be related to the electrostatic potentials at the site of the donor and acceptor ions. For the purpose of comparison of our Car-Parrinello results to classical model studies it is instructive to take a more detailed look at the vertical gap in the simple point charge approximation. The total energy in such a model can be written (in atomic units) as

$$U_{\mathrm{A}}\left(\mathbf{R}^N\right) = \frac{q_{\mathrm{D}}q_{\mathrm{A}}}{r_{\mathrm{DA}}} + \sum_{i}^{solvent}\left(\frac{q_{\mathrm{D}}q_i}{r_{\mathrm{D}i}} + \frac{q_{\mathrm{A}}q_i}{r_{\mathrm{A}i}}\right) + \sum_{i>j}^{solvent}\frac{q_iq_j}{r_{ij}} + \sum_{i>j}^{N} v_{ij}\left(r_{ij}\right) \quad (6)$$

where the charges and positions of the donor and acceptor ion are labeled by the subscript D respectively A and i counts solvent particles. v_{ij} is some atom-atom potential describing short range interactions between particles i and j. Summation for this pair interaction term runs over all particles N in the model (solutes plus solvent) where the donor particle D is now identified with the particle with index $i = 1$ and the acceptor with the particle indicated by index $i = 2$. If we assume that q_{D} and q_{A} are the charges of donor and acceptor in the reactant state we can interpret the energy U_{A} of (6) as the total energy before the transfer, hence the subscript A. The charge of donor and acceptor after the transfer will then be $q_{\mathrm{D}}+1$ respectively $q_{\mathrm{A}}-1$ and the total energy U_{B} of the product becomes

$$U_{\mathrm{B}}\left(\mathbf{R}^N\right) = \frac{\left(q_{\mathrm{D}}+1\right)\left(q_{\mathrm{A}}-1\right)}{r_{\mathrm{DA}}} + \sum_{i}^{solvent}\left(\frac{q_{\mathrm{D}}+1}{r_{\mathrm{D}i}} + \frac{q_{\mathrm{A}}-1}{r_{\mathrm{A}i}}\right)q_i + \sum_{i>j}^{solvent}\frac{q_iq_j}{r_{ij}} + \sum_{i>j}^{N} v_{ij}\left(r_{ij}\right) \quad (7)$$

Subtracting gives the vertical energy gap.

$$\Delta U = U_{\mathrm{B}} - U_{\mathrm{A}} = \frac{\left(q_{\mathrm{A}} - q_{\mathrm{D}} - 1\right)}{r_{\mathrm{DA}}} + \sum_{i}^{solvent}\left(\frac{1}{r_{\mathrm{D}i}} - \frac{1}{r_{\mathrm{A}i}}\right)q_i \quad (8)$$

$$= -\frac{1}{r_{\mathrm{DA}}} + \sum_{i\neq 1}^{N}\frac{q_i}{r_{\mathrm{D}i}} - \sum_{i\neq 2}^{N}\frac{q_i}{r_{\mathrm{A}i}} \quad (9)$$

All short range interaction cancel since the position of the particles are kept fixed during a vertical transfer. Recalling that the electrostatic potential at the site of a particle i can be expressed as

$$\Phi_i\left(\mathbf{R}^N\right) = \sum_{j\neq i}^{N}\frac{q_j}{r_{ij}} \quad (10)$$

we recognize in the last two terms of (9) the difference of the electrostatic potentials acting on the donor ($i = 1$) and acceptor ($i = 2$) and we can write the point charge gap as

$$\Delta U\left(\mathbf{R}^N\right) = -\frac{1}{r_{\mathrm{DA}}} + \Phi_{\mathrm{D}}\left(\mathbf{R}^N\right) - \Phi_{\mathrm{A}}\left(\mathbf{R}^N\right) = -\frac{1}{r_{\mathrm{DA}}} + IP_{\mathrm{D}} - EA_{\mathrm{A}} \quad (11)$$

Equation (11) is indeed equal to the vertical electron transfer excitation energy (4) in the classical point charge approximation (plus weak coupling limit). This is made explicit in the second identity, where IP_{D} is the ionization potential of the donor and EA_{A} the electron affinity of the acceptor. The first term is the direct "particle-hole" Coulomb contribution to the excitation energy.

2.2 Reaction Free Energies

The crucial step, as in any study of chemical reactivity based on reaction coordinates, is the computation of the free energy profile or potential of mean force (PMF). A formalism with separately defined potential energy surfaces for reactant A (see Sect. 2.1) and product B also yields two separate diabatic free energy profiles. So, to begin with the total free energy we define

$$A_M = -k_\mathrm{B}T \ln \Lambda^{-3N} \int \mathrm{d}\mathbf{R}^N \exp[-\beta E_M\left(\mathbf{R}^N\right)] \tag{12}$$

where $M = \mathrm{A}, \mathrm{B}$. E_A is the diabatic PES of state A, and E_B the PES of state B (3). Λ is the average thermal wavelength of the atoms defined as $\Lambda^{-3N} = \prod_j \lambda_j^{-3N_j}/N_j!$ with $\lambda_j = h/\sqrt{2\pi m_j k_\mathrm{B} T}$ the thermal wavelength of the nuclear species j. As usual $\beta^{-1} = k_\mathrm{B}T$ with k_B the Boltzmann constant and T the temperature. The reaction free energy change can then be related to a ratio of partition functions

$$\Delta A = A_\mathrm{B} - A_\mathrm{A} = -k_\mathrm{B}T \ln \frac{\int \mathrm{d}\mathbf{R}^N \exp(-\beta\, E_\mathrm{B}\left(\mathbf{R}^N\right))}{\int \mathrm{d}\mathbf{R}^N \exp(-\beta\, E_\mathrm{A}\left(\mathbf{R}^N\right))} \tag{13}$$

Note that a definition of order parameters distinguishing between reactant and product is not needed. Integration in (12) and (13) extends over the full configuration space.

Next the free energy profile. Unlike the total free energy (12), this quantity is not unique. It does depend on the specification of an order parameter $X\left(\mathbf{R}^N\right)$. This can be a geometric characteristic such as bond length or angle, or, what we are going to use in the end, the vertical energy gap $\Delta E\left(\mathbf{R}^N\right)$. The definition of the diabatic free energy profiles $A_M(x), M = \mathrm{A}, \mathrm{B}$ is similar to (12) but now the integral is restricted to atomic configurations having a given value x of the function $X\left(\mathbf{R}^N\right)$. The restriction is formally imposed by inserting a Dirac delta function.

$$A_M(x) = -k_\mathrm{B}T \ln \Lambda^{-3N} \int \mathrm{d}\mathbf{R}^N \exp[-\beta E_M\left(\mathbf{R}^N\right)]\delta(X\left(\mathbf{R}^N\right) - x) \tag{14}$$

The probability distribution for x can be defined by a similar integral normalizing by the full unrestricted partition function

$$p_M(x) = \frac{\int \mathrm{d}\mathbf{R}^N \exp[-\beta E_M\left(\mathbf{R}^N\right)]\delta(X(\mathbf{R}^N) - x)}{\int \mathrm{d}\mathbf{R}^N \exp[-\beta E_M\left(\mathbf{R}^N\right)]} = \langle \delta\left(X - x\right)\rangle_M \tag{15}$$

In the second identity the probability distribution is formally written as an expectation value of a Dirac delta function (recall the difference in status of X and x in our notation, X is a function of configuration $\mathbf{R}^N$, which has been suppressed here, while x is a constant). Comparing (14) and (15) we see that

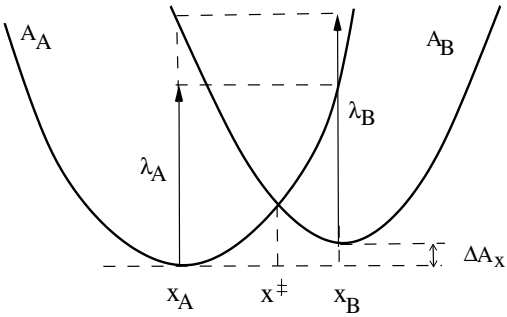

Fig. 2. Two intersecting diabatic free energy surfaces A_A and A_B (*thick solid curves*). *Thin solid arrows* represent the reorganization free energies λ_A and λ_B as defined in (17) and (18). Also indicated is the reaction free energy change ΔA_x of (19). Note the important difference with Fig. 1 which shows potential energy curves E_M and vertical energy gaps ΔE. The aim of the theory in this review (Marcus theory) is to establish a relation between energy gaps and free energies

$$A_M(x) = -k_\mathrm{B}T \ln p_M(x) + A_M \tag{16}$$

where A_M is the diabatic free energy of (12). The free energy profiles (14) are the basis for the definition of reorganization and activation free energies, using (16) for their computation. These free energies are differences relative to the values of the stable minimum of $A_M(x)$ in the reactant and product state. We will indicate the location of these minima by x_A and x_B (see Fig. 2). Reorganization free energies are then defined as

$$\lambda_\mathrm{A} = A_\mathrm{A}\left(x_\mathrm{B}\right) - A_\mathrm{A}\left(x_\mathrm{A}\right) \tag{17}$$

$$\lambda_\mathrm{B} = A_\mathrm{B}\left(x_\mathrm{A}\right) - A_\mathrm{B}\left(x_\mathrm{B}\right) \tag{18}$$

While reorganization free energies for reactant and product state are in general different, $\lambda_\mathrm{A} = \lambda_\mathrm{B}$ in Marcus theory (see Sect. 2.4). We should also be careful to distinguish between the reaction free energy change as determined from the stable values of $A_M(x)$ (see Fig. 2)

$$\Delta A_x = A_\mathrm{B}\left(x_\mathrm{B}\right) - A_\mathrm{A}\left(x_\mathrm{A}\right) \tag{19}$$

and the reaction free energy ΔA of (13). ΔA_x of (19) is, in principle, dependent on the choice of reaction coordinate, which is why we have appended the subscript x, while ΔA of (13) is not. Finally the free energy of activation for the forward ($M = \mathrm{A}$) and reverse ($M = \mathrm{B}$) reaction can be defined as

$$\Delta A^\dagger_M = A_M\left(x^\dagger\right) - A_\mathrm{M}\left(x_\mathrm{M}\right) \tag{20}$$

where $x^\dagger$ is the value of the reaction coordinate where the diabatic curves intersect.

2.3 Free Energy Perturbation Method

The gap is a difference of total energies. The free energy required to change the gap can therefore be obtained using free energy perturbation methods developed in classical force field based simulation to calculate the free energy cost of a modification of the Hamiltonian (see [40, 41] and the text book of Frenkel and Smit [42]). This special feature of the gap has a number of consequences, both from the point of view of computational method [5, 7] and interpretation [10]. We start by noting that the expression (13) can be rewritten as an average over the exponential of the vertical energy gap ΔE of (3). The result has the form of a free energy perturbation (FEP) expression [40–42]

$$\Delta A = -\frac{1}{\beta} \ln\langle e^{-\beta \Delta E} \rangle_{\mathrm{A}} \tag{21}$$

$$= \frac{1}{\beta} \ln\langle e^{\beta \Delta E} \rangle_{\mathrm{B}} \tag{22}$$

where $\langle \cdots \rangle_M$ denotes the canonical average over the PES of state $M = \mathrm{A,B}$. As profound as this expression is, it is also impossible to use in practical calculations, except in very special cases. The reason is that for most systems of interest there is no overlap between regions in configuration space accessible by thermal fluctuations of the equilibrium reactant and product. So, taking (21) as example, the configurations visited by a trajectory in state A will give large positive values for ΔE and therefore a vanishing exponential weight (see Fig. 1). On the other hand ΔE is negative for equilibrium configurations of state B resulting in a huge exponent. Unfortunately the dynamics controlled by E_{A} never reaches this part of configuration space. A sure signature of these sampling problems is a discrepancy between the averages of (21) and (22).

The reader should be familiar with the problem. It is the central problem in free energy computation which every method is trying to solve. The method favored by Warshel in his ET calculations (for a review see [7]) is umbrella sampling (US) using as biasing potential a linear superposition of the two diabatic PES:

$$E_\eta\left(\mathbf{R}^N\right) = \eta E_{\mathrm{B}}\left(\mathbf{R}^N\right) + (1-\eta) E_{\mathrm{A}}\left(\mathbf{R}^N\right) \tag{23}$$

Varying the value of the coefficient η from 0 to 1 creates a series of potentials gradually transforming E_{A} into E_{B}. The discrete increments $\Delta\eta$ must be chosen sufficiently small for the exponential sampling to be accurate so we can use (21) to estimate the corresponding increase in free energy

$$A(\eta + \Delta\eta) - A(\eta) = -k_{\mathrm{B}} T \ln\langle \exp\left[-\beta\left(E_{\eta+\Delta\eta} - E_\eta\right)\right]\rangle_\eta \tag{24}$$

where $A(\eta) = -k_{\mathrm{B}} T \ln \Lambda^{-3N} \int \mathrm{d}\mathbf{R}^N \exp(-\beta E_\eta)$ is the free energy generated by the surface E_η (conf. (12)) and the subscripted brackets denote a thermal average over this surface. The reaction free energy ΔA is obtained by

adding all intermediate free energy changes. Alternatively we can exploit the linear dependence on η which goes back to the coupling parameter method of Kirkwood [43] and use thermodynamic integration

$$\Delta A = A(1) - A(0) = \int_0^1 \mathrm{d}\eta \, \frac{\mathrm{d}A(\eta)}{\mathrm{d}\eta} = \int_0^1 \mathrm{d}\eta \, \langle \Delta E \rangle_\eta \tag{25}$$

Similar to (24) $\langle \Delta E \rangle_\eta$ is computed for a discrete set of values of η (windows) between 0 and 1 and the integral is approximated by a finite sum.

The extension of the FEP/US scheme for the computation of the order parameter probability function $p_M(x)$ (15) is an example of the histogram method. $p_M(x)$ can be obtained in "principle" by determining a histogram of order parameter fluctuations in state M. However, what we are interested in, is the value of $p_M(x)$ at the crossing of the diabatic free energy surfaces $A_\mathrm{A}(x)$ and $A_\mathrm{B}(x)$ because that is where the reaction (electron transfer) takes place. This will give us our estimate of the activation free energy (see Fig. 2 and below). But, of course, we encounter the same problem as for reaction free energy change calculation, this region will be out of reach of equilibrium fluctuations and is sampled very poorly, if at all. This is no different from the adiabatic picture. However, the diabatic picture (an approximation justified in the weak coupling limit) allows for a neat formulation of this problem. Following a derivation similar to the one which led to (21), we can relate the order parameter probability distributions of one diabatic state to the distribution of the other.

$$\frac{p_\mathrm{B}(x)}{p_\mathrm{A}(x)} = e^{\beta \Delta A} \frac{\langle e^{-\beta \Delta E} \delta(X - x) \rangle_\mathrm{A}}{\langle \delta(X - x) \rangle_\mathrm{A}} \tag{26}$$

As in (21) we have to include exponents of the vertical gap as weights in the averaging. This seriously deteriorates the accuracy except when the energy differences are small, such as is the case in the crossing region where the weights are approximately unity ($\Delta E \approx 0$). So the idea is again to bridge distributions p_A and p_B by a series of overlapping distributions (umbrellas) generated by the bias potential (23). The fluctuations of $X\left(\mathbf{R}^N\right)$ for the MD trajectories for a representative set of discrete values of η are binned in histograms. These histograms are merged into a single diabatic probability distribution $p_\mathrm{A}(x)$ which now extends all the way to values of x where $p_\mathrm{B}(x)$ has its maximum (see for example [44] and the Frenkel & Smit textbook [42]).

Equation (26) also shows why the vertical energy gap ΔE is different from other reaction coordinates. Taking logarithms and substituting (16) we find

$$A_\mathrm{B}(x) - A_\mathrm{A}(x) = -k_\mathrm{B} T \ln \left[\frac{\langle e^{-\beta \Delta E} \delta(X - x) \rangle_\mathrm{A}}{\langle \delta(X - x) \rangle_\mathrm{A}} \right] \tag{27}$$

Setting $\Delta E = X$ we see that ΔE appears both in the argument of the delta function on the rhs and the exponent. As a result the exponent can be taken outside the configurational integral giving

$$A_{\mathrm{B}}(\epsilon) - A_{\mathrm{A}}(\epsilon) = \epsilon \tag{28}$$

where ϵ stands for a given value of the gap ΔE. This relation, commonly referred to as the Zwanzig relation, states that the logarithm of the probability distributions of the diabatic states are linearly dependent. The free energy curve of the product can be obtained adding ϵ to the free energy curve for the reactant. This equation, which is rigorous and completely general has a number of interesting and useful implications for computations which use the energy gap as reaction coordinate. For example, substituting in (17) and (18) with $X = \Delta E$ we find for the reorganization energies

$$\lambda_{\mathrm{A}} = +\Delta A_{\epsilon} - \epsilon_{\mathrm{B}} \tag{29}$$

$$\lambda_{\mathrm{B}} = -\Delta A_{\epsilon} + \epsilon_{\mathrm{A}} \tag{30}$$

where ΔA_{ϵ} is the reaction free energy change as determined from the minima in the $A_M(\epsilon)$ curves at ϵ_{A} and ϵ_{B} (see (19)). Equations (29) and (30) tell us that, once we have an estimate of the reaction free energy change, we can find the reorganization free energies simply from the equilibrium values of the diabatic gap, which for all practical purposes can be equated with the average gap in the reactant and product state. This is particularly helpful when the reaction free energy change vanishes ($\Delta A_{\epsilon} = 0$), as for example for self exchange reactions. Note also that, since reorganization free energies are by definition positive, (29) and (30) imply that

$$\epsilon_{\mathrm{B}} < \Delta A_{\epsilon} < \epsilon_{\mathrm{A}} \tag{31}$$

The equilibrium energy gaps set a lower and upper bound to the reaction free energy change. Finally, since in the diabatic approximation the transfer is assumed to take place at the curve crossing ($\epsilon^{\dagger} = 0$), the activation free energy (20) becomes directly equal to the free energy cost of closing the energy gap,

$$\Delta A_M^{\dagger} = A_M\left(\epsilon = 0\right) - A_M\left(\epsilon_M\right) \tag{32}$$

2.4 Relation to Marcus Theory

We are now ready to return to Marcus theory, which was at the origin of all this formalism. Marcus assumed that the solvent responds linearly to a change in charge, which is equivalent to approximating distribution (15) for the energy gap by a Gaussian

$$p_M(\epsilon) = \frac{1}{\sqrt{2\pi}\sigma_M} \exp\left[-(\epsilon - \epsilon_M)^2/(2\sigma_M^2)\right], \tag{33}$$

where $M = \mathrm{A}, \mathrm{B}$. Since we are dealing with Gaussians

$$\epsilon_M = \langle \Delta E \rangle_M \tag{34}$$

Similarly the squared widths σ_M^2 in (33) are equal to the variance of the gap fluctuations

$$\sigma_M^2 = \left\langle \left(\Delta E - \langle \Delta E \rangle_M \right)^2 \right\rangle_M \tag{35}$$

The corresponding free energy profiles (16) are parabolic

$$A_M(\epsilon) = A_M^\epsilon + \frac{k_\mathrm{B}T}{2\sigma_M^2} \left(\epsilon - \epsilon_M \right)^2 \tag{36}$$

As pointed out in Sect. 2.2 the minimum free energy A_M^ϵ and the total free energy of A_M of (12) are not the same. For Gaussian distributions it is easy to find what is missing

$$A_M^\epsilon = A_M + \frac{k_\mathrm{B}T}{2} \ln \left[2\pi\sigma_M^2 \right] \tag{37}$$

Now comes the step where we use (28) which is special to energy gaps. According to this equation, free energy functions for vertical gaps can differ only by a linear term. This means that quadratic terms must cancel which can only be satisfied if the variance of the fluctuations is independent of the chemical state of the system

$$\sigma_\mathrm{A}^2 = \sigma_\mathrm{B}^2 \equiv 2k_\mathrm{B}T\lambda' \tag{38}$$

The second identity defines the linear response reorganization free energy λ'. Equation (38) may at first seem a rather strong claim, in particular for half reactions, but is, according to (28), a rigorous consequence of the Gaussian approximation. Any violation of this relation must be due to non-linearities as was pointed out by Tachiya in [45]. Similarly, λ' in (38) is in general not identical to the reorganization free energies of (29) and (30) (which is why we have added the prime). This is another point emphasized by Tachiya [39]. For Gaussian distributions, however, these quantities are indeed the same. This follows from the constraints imposed by (28) on the linear coefficients in (36) which require

$$\lambda' = \frac{1}{2} \left(\epsilon_\mathrm{A} - \epsilon_\mathrm{B} \right) \tag{39}$$

Substituting with (36) in expression (29) for λ_A we obtain

$$\lambda_\mathrm{A} = \frac{1}{4\lambda'} \left(\epsilon_\mathrm{A} - \epsilon_\mathrm{B} \right)^2 = \lambda' \equiv \lambda \tag{40}$$

The same result is found for λ_B of (30). For parabolic free energy curves of energy gaps we can therefore forget about the various kinds of reorganization energy, there is only one, which we call λ. Similarly, because of (38) and (37) we can conclude that in the Gaussian approximation the discrepancy between the reaction free energies of ΔA (13) and ΔA_ϵ of (19) vanishes. Rearrangement of (29) and (30) then yields two very useful relations between equilibrium Gaussian energy gaps and the reaction and reorganization free energies

$$\Delta A = \frac{1}{2}\left(\epsilon_{\mathrm{A}} + \epsilon_{\mathrm{B}}\right) \tag{41}$$

$$\lambda = \frac{1}{2}\left(\epsilon_{\mathrm{A}} - \epsilon_{\mathrm{B}}\right) \tag{42}$$

Note that (41) can be directly obtained from the two point approximation to the coupling parameter integral (25). Yet another route to (41) and (42) departs from the cumulant expansion of (21) and (22) (see e.g. [31]).

$$\Delta A = \langle \Delta E \rangle_{\mathrm{A}} - \frac{1}{2k_{\mathrm{B}}T}\sigma_{\mathrm{A}}^2 = \langle \Delta E \rangle_{\mathrm{B}} + \frac{1}{2k_{\mathrm{B}}T}\sigma_{\mathrm{B}}^2 \,, \tag{43}$$

For Gaussian statistics truncation after the second term is exact. Inserting (34) and (38), we can recover (41) by adding and (42) by subtracting. Equations (43) and (38) are the ultimate of economy in free energy computation. While (41) and (42) require two equilibrium runs (one for reactant and one for the product), (43) and (38) claim that both ΔA and λ can be obtained from the mean and variance of the gap fluctuations of a single trajectory, either reactant or product state. The trajectory must of course be of sufficient length to converge the variance σ_M^2. This quantity has been eliminated in (41) and (42) which is a significant advantage in *ab initio* MD calculations, where runs are short. Finally, substitution in (32) yields the famous Marcus gap law for the activation energy (written here for the forward reaction)

$$\Delta A_{\mathrm{A}}^{\dagger} = \frac{(\lambda + \Delta A)^2}{4\lambda} \tag{44}$$

3 Redox Half Reactions

3.1 Ab Initio MD Considerations

Equations (29), (30) and (32), or their Gaussian (Marcus) approximations of Sect. 2.4, have been the basis for much of the simulation work on electron transfer, using either semiclassical methods or fully classical point charge models. However, the use of the vertical diabatic energy gap as a reaction coordinate is not restricted to ET in the weak coupling limit even though for systems with strong off-diagonal interactions (1) the diabatic energy surfaces are not acceptable approximations to the adiabatic PES. The discrepancies, particularly in the crossing region, are too large. However, while ΔE can no longer be interpreted as the vertical (optical) ET excitation energy (4), it retains its usefulness as an order parameter for ET. Moreover, the diabatic PES can be used as a reference potential. The deviation from the true adiabatic ground state energy surface can be accounted for by means of FEP techniques similar to the methods discussed in Sect. 2.3. The adiabatic ground state energy can be obtained from diagonalization of the diabatic Hamiltonian matrix ((1) in case of a two level model) or from a completely independent calculation

using ab initio electronic structure methods such as MP2 or DFT [8,9]. The question then is how to define the diabatic PES. Warshel and coworkers opt for an empirical valence bond (EVB) scheme. In a series of papers they have applied this approach, not only to ET [5–7] but also to proton transfer and enzymatic reactions [8–11].

How to implement the diabatic energy gap approach in a DFT based ab initio MD ("Car-Parrinello") simulation of a condensed molecular system, when there is no EVB model available? In the case of ET it should be in principle feasible to reconstruct the diabatic surfaces from the adiabatic electron transfer excitation energies. Unfortunately DFT, at the level it is usually applied in ab initio MD simulation, is notoriously unreliable for treating charge transfers. The way we have avoided this problem in our work on redox reactions is to separate full redox reactions (2) in half reactions.

$$\mathrm{R} \rightarrow \mathrm{O} + \mathrm{e}^- \tag{45}$$

Model systems now consist only of a single redox active solute rather than two. Instead the number of electrons in the system can vary between n, say, for the reduced state R and $n-1$ for the oxidized state O. Implementation in a Car-Parrinello simulation is fairly straightforward. The method normally produces a finite temperature trajectory on the adiabatic ground state PES of R or O. What our scheme in essence does is adding a second calculation recomputing for the same ionic configuration the ground state energy of the system with one electron less, (O) or one electron more (R), which gives the vertical energy gap at that configuration.

The non-adiabatic picture as expressed in (5) is thus taken to the extreme in our half reaction scheme. The coupling parameter γ is not only small, it is zero, as it would be the case for very large separations between donor and acceptor. This is in fact the proper limit for the reaction free energy ΔA if we want to compare the result of our calculations to experimental *standard* redox potentials which formally correspond to reaction free energies at infinite dilution. This is the main objective of our approach. However, also the activation and reorganization free energies remain meaningful, if not quantitatively, then at least qualitatively as a way to understand the redox reaction kinetics.

There is, however, a serious objection that comes immediately to mind. The interpretation of the vertical gap ΔE or free energy ΔA as the corresponding quantities in a homogeneous solution clearly cannot be correct in model systems under periodic boundary conditions as used in our simulation. Either the R or O state, or both, end up with a net charge. In the Ewald summation methods used in our codes, net charge of the model is automatically compensated by a homogeneous back ground charge, effectively playing the role of a counter ion. Energies of half reactions have therefore no experimental meaning. Still, free energies of full reactions, obtained as differences of half reactions, can be compared to experiment, but only if charges of reactant and product species are the same. Under these (rather restrictive) conditions long

range interactions cancel (see Sect. 4.1). System size effects are not the subject of this contribution which focuses on the statistical mechanics. The practical justification we can offer here is the success of our scheme in reproducing a (limited) number of experimental redox potentials for full reactions of model aqueous transition metal coordination complexes and organic molecules (see further Sect. 4.1).

3.2 Parallel to Electrode Reactions

There is a second way to view the half reaction scheme. In electrochemistry a half reaction (45) is regarded as a zero order approximation to heterogeneous electron transfer between an ion in solution and a metal electrode E (see for example [46]). In the notation used in previous sections where reactant and product state were indicated by A respectively B, we now have A = R + E representing the state with the electron held by the reduced ion and B = O + E^- the state with the active electron transferred to the electrode E. This is a very useful parallel. It suggests that the thermodynamic driving force in the simulation can be controlled similar to the way electrochemists control a redox reaction by applying a voltage to the electrodes of the cell. In the minimal implementation of this scheme we have employed in our simulations, the electrode is replaced by a fictitious electron reservoir at electronic chemical potential μ, which exchanges electrons with the solution but has no further interactions with the solution. The PESs A and B remain the same in this approximation except that we must add a shift μ to the PES of B

$$E_{\mathrm{A}}\left(\mathbf{R}^N\right) = E_{\mathrm{R}}\left(\mathbf{R}^N\right) \tag{46}$$

$$E_{\mathrm{B}}\left(\mathbf{R}^N\right) = E_{\mathrm{O}}\left(\mathbf{R}^N\right) + \mu \tag{47}$$

The vertical energy gap (3) for the transfer to the fictitious electrode is offset by the same bias μ. We formally write for this electrochemically controlled gap

$$\Delta E_{\mu}\left(\mathbf{R}^N\right) = E_{\mathrm{B}}\left(\mathbf{R}^N\right) - E_{\mathrm{A}}\left(\mathbf{R}^N\right) = \Delta E\left(\mathbf{R}^N\right) + \mu \tag{48}$$

where ΔE is the ET energy of (3). The same linear relation holds for the free energy of oxidation

$$\Delta A_{\mu} = A_{\mathrm{B}} - A_{\mathrm{A}} = \Delta A + \mu \tag{49}$$

where ΔA is the free energy difference (13). This will be the interpretation of (45) we adopt in the remainder of the discussion. All equations of Sects. 2.2, 2.3 and 2.4 can be carried over if we make the following simple replacements

$$\begin{aligned} \mathrm{A} &\rightarrow \mathrm{R} & \mathrm{B} &\rightarrow \mathrm{O} \\ \Delta E &\rightarrow \Delta E_{\mu} & \Delta A &\rightarrow \Delta A_{\mu} \end{aligned} \tag{50}$$

In practice the electrochemical potential μ plays the role of an external parameter used to align the free energy profiles of reactant and product state.

Indeed by choosing $\mu = -\Delta A$ the effective reactive energy change ΔA_μ (49) can be made to vanish. ΔA can be estimated using the FEP methods outlined in this chapter or alternatively, we can use the "numerical titration scheme" proposed in [34] and applied in [28] and [31]. The freedom of the control over μ is directly exploited in this scheme by stepwise variation of μ until the oxidation reaction is observed (for a critical evaluation of this approach and a comparison to the FEP method see [31]).

4 Applications

4.1 Overview

The methodology outlined in the previous sections has been applied to a number of redox active solutes. The redox reactions we have investigated and the result for the reaction free energy change are listed in Table 1 together with the experimental values of the reaction free enthalpy. The density functional in all calculations was BLYP. The simulation for the aqueous transition metal coordination complexes (reactions **1** and **2**) were carried using the CPMD package [47]. Standard norm conserving pseudo potentials (Trouillier-Martins [48]) were used and conventional plane wave cutoffs ($70 - 80$Ry). Technical details can be found in the original publications given in Table 1. For the molecular systems (reactions **3** and **4)** we employed a new mixed Gaussian-plane wave *ab initio* MD method [49] and the Quickstep code [50]. The one electron orbitals are expanded in Gaussian basis sets. Core electrons are represented using separable norm conserving pseudo potentials according to the Goedecker-Hutter recipe [51]. The plane waves are used as an auxiliary basis set to describe the density [49] which enables us to compute the long range electrostatic energies using fast Fourier transform methods similar to CPMD.

Table 1. Reaction free energies in units of eV of four model redox reactions compared to experiment. The first two reactions involve transition metal aqua ions. TH (thianthrene) and TTF (tetrathiafulvalene) are two organosulfur compounds which can be oxidized to stable radical cations. BQ (benzoquinone) and DQ (duroquinone) are small quinones forming radical anions. The last column gives the reference to the original papers

	Redox Reaction	Solvent	ΔA(calc.)	ΔG(exp.)	Ref.
(**1**)	$Cu^{1+} + Ag^{2+} \rightarrow Cu^{2+} + Ag^{1+}$	water	-1.7	-1.83	28
(**2**)	$RuO_4^{2-} + MnO_4^{1-} \rightarrow RuO_4^{1-} + MnO_4^{2-}$	water	-0.3	$+0.03$	31
(**3**)	$TH^{\bullet+} + TTF \rightarrow TH + TTF^{\bullet+}$	acetonitrile	-0.9	-0.93	35
(**4**)	$DQ^{\bullet-} + BQ \rightarrow DQ + BQ^{\bullet-}$	methanol	-0.43	-0.46	36

The redox free energies ΔA of reactions **2, 3** and **4** were estimated from the average vertical energy gaps using the Marcus approximation ((41) for reactions **2** and **3** and (43) for reaction **4**). ΔA of reaction **1** was obtained using the scheme of [34]. This method for the determination of redox potentials does not have to rely on the Gaussian approximation and can be applied to systems outside the Marcus regime. The Ag ion [33] and most likely also the Cu aqua ion are examples of such non-Marcus ions (see further Sect. 4.2).

The agreement with experiment is good. Discrepancies are in the 100 meV range except for reaction **2**, where the error is 300 meV. The simulation parameters most critical to the assessment of the accuracy of these results are the duration of the MD runs and the model system size. The typical run length is 10 ps (some runs are shorter, 5 ps, others longer, 20 ps). The number of solvent molecules is between 30 and 50, with cubic box dimensions in the order of 10-15 Å. All model systems contain only a single redox active ion without counterion. In systems of such small dimensions the interaction with periodic images and the Ewald back ground charge distribution is very large (in the eV's). There are a number of considerations why these large size effects are apparently not affecting the accuracy of the redox free energies in Table 1 to the same extent. Most important is a compensation of errors. The reactions in Table 1 are all of the type

$$\mathrm{X}^m + \mathrm{Y}^{m+1} \rightarrow \mathrm{X}^{m+1} + \mathrm{Y}^m \tag{51}$$

The species in reactant and product have the same charges and approximately the same spatial dimension. From a distance they will look rather similar to the solvent and the long range errors cancel.

4.2 Two Examples: The Ru and Ag Aqua Cations

As an illustration of the methods presented in this chapter, and to underline the importance of vertical energy gaps, we will discuss two half reactions in more detail. Both involve transition metal aqua cations. The first is the $\mathrm{Ag}^{1+} \rightarrow \mathrm{Ag}^{2+} + e^-$ oxidation, i.e. half of the reaction **1** of Table 1. The second is $\mathrm{Ru}^{2+} \rightarrow \mathrm{Ru}^{3+} + e^-$. The reason that this reaction is not included in Table 1 is that we have not yet studied another metal ion with reduced and oxidized states of the same charge so as to satisfy (51). The subject of the discussion in this section is however not the redox free energy itself but the statistical mechanics of the vertical energy gap. We have used therefore the freedom of the control of the redox free energy (49), by choosing a value of μ such that $\Delta A_\mu = 0$. This effectively aligns the free energy minima of the diabatic surfaces in Fig. 2. These values of μ, which are different for each reaction, are given in the caption of Fig. 3 (recall again that similar to ΔA of half reactions, values of μ have no direct experimental meaning).

The probability distributions (15) of the (shifted) vertical energy gap of (48) are shown in Fig. 3. These distributions have been determined by sampling the time evolution of the vertical gap ΔE_μ in equilibrium runs of reduced

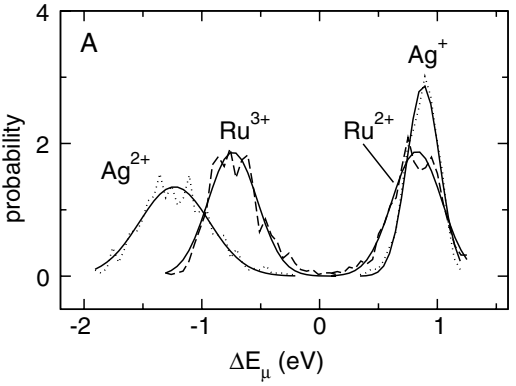

Fig. 3. Vertical energy gap probability distributions p_M (15) as determined from equilibrium trajectories for two oxidation states of the Ru and Ag aqua-cations. *Dashed* and *dotted lines* are the original histograms, *solid curves* are Gaussian fits. The oxidation free energy ΔA has been set to zero by choosing the appropriate value for the chemical potential, $\mu = 0.58$ eV for Ru^{2+}/Ru^{3+} and $\mu = -1.16$ eV for Ag^{1+}/Ag^{2+}. Note the asymmetry for the Ag system (see also Table 2)

and oxidized state. We immediately notice a difference. The distributions for Ru are to a very good approximation Gaussian. The distribution for reduced state (p_R) and oxidized state (p_O) are placed in symmetrical position relative to $\Delta E_\mu = 0$ and have the same variance (see Table 2). This is in agreement with (38) and (41), which requires that $\epsilon_O = -\epsilon_R$ for $\Delta A = 0$ (converting the notation according to (50)). As explained in Sect. 2.4 this symmetry is a necessary condition a Gaussian system must fulfill. Indeed the ET chemistry of

Table 2. Properties characterizing the diabatic free energy profiles A_M shown in Fig. 4 for the Ru^{2+}/Ru^{3+} couple and Fig. 5 for Ag^{1+}/Ag^{2+}. The parameter ϵ_M gives the location of the position of the minimum of the parabolic fit to A_M and λ_M the reorganization free energy computed from these fits according to (17) and (18). $\Delta A^\dagger$ is the activation free energy determined from the intersection point of the parabolic curves. The order parameter is the quantum energy gap of (48) except for the data marked as Ru^{2+}/Ru^{3+}(cl.) which refer to the classical point charge gap of (53). The widths σ_M are the root mean square second moments (35) of the corresponding gap fluctuations used in the criterion of (38) to decide whether Marcus theory applies. All energies are in eV. Data are taken from [32] and [33]

	ϵ_R	ϵ_O	σ_R	σ_O	λ_R	λ_O	$\Delta A^\dagger$	Fig.
Ru^{2+}/Ru^{3+}	0.78	-0.78	0.23	0.23	0.78	0.78	0.20	4A
Ru^{2+}/Ru^{3+}(cl.)	1.00	-0.82	0.39	0.33	0.24	0.42	0.08	4B
Ag^{1+}/Ag^{2+}	1.17	-1.20	0.14	0.30	1.19	1.15	0.3	5

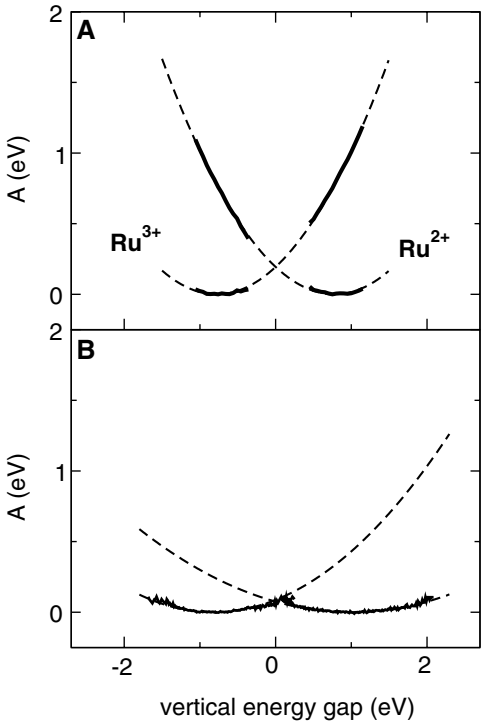

Fig. 4. A: Free energy profiles for Ru^{2+} and Ru^{3+} corresponding to the probability distributions of Fig. 3 using the shifted vertical energy gap of (48) as order parameter. The low energy set of points have been obtained according to (16). The upper parts have been obtained from the lower parts by adding or subtracting the energy gap using (28). Dashed curves are parabolic fits. Panel **B** shows the free energy profiles obtained using the fluctuations of the classical point charge gap of (53) (data taken from [32])

Ru cations is a text book example of an outer sphere process to which Marcus theory applies. Ru(II) forms an octahedral coordination complex with water, $Ru(II)(H_2O)_6$, which is, apart from a small contraction of the metal oxygen distance, virtually preserved in oxidation state III (radial distribution functions and other geometry data can be found in [32]). In contrast Ag^{1+}/Ag^{2+} shows a significant asymmetry. This is consistent with the substantial changes in the hydration structure induced by oxidation. As we found in [28] the coordination number of Ag^{1+} is on average 4 (fluctuations are however large) while the coordination number of Ag^{2+} is 5 (see also [29] and [33]). This coordination change increases the importance of non-linear effects which would violate the assumptions for the validity of the Gaussian approximation (Sect. 2.4).

The free energy profiles corresponding to the distributions of Fig. 3 are shown in Fig. 4 (upper panel) for Ru^{2+}/Ru^{3+} and for Ag^{1+}/Ag^{2+} in Fig. 5.

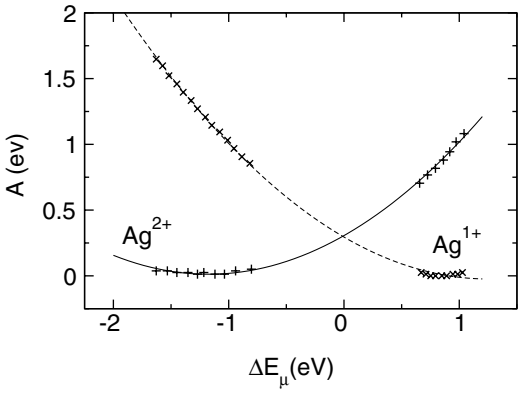

Fig. 5. Free energy profiles for Ag^{1+} ($\times$ symbols) and Ag^{2+} (+ symbols) corresponding to the probability distributions of Fig. 3. The low energy set of points have been obtained according to (16). The upper parts have been obtained from the lower parts using (28). The solid and dashed curves are parabolic fits (data taken from [33])

The curve for each oxidation state consists of two sets of data points connected by a parabolic fit (thin lines). The data points have been obtained as follows. The lower energy part of $A_{\mathrm{R}}(\epsilon)$ has been computed from $p_{\mathrm{R}}(\epsilon)$ by taking the logarithm according to (16) and setting the constant A_{R} to zero. The low energy part of $A_{\mathrm{O}}(\epsilon)$ has been computed applying the same procedure to $p_{\mathrm{O}}(\epsilon)$. In contrast the high energy part of $A_{\mathrm{R}}(\epsilon)$ (at negative gap values) has been obtained from the equilibrium trajectory of the O state. Using (28) we have simply subtracted the value of the vertical gap from $A_{\mathrm{O}}(\epsilon)$. The part of $A_{\mathrm{O}}(\epsilon)$ at positive gap values was generated from $A_{\mathrm{R}}(\epsilon)$ in a similar way.

As expected the free energy profiles of Ru^{2+}/Ru^{3+} form a mirror pair of intersecting diabatic curves. The positions of the minima as obtained from the parabolic fits are listed in Table 2 (first row) which also gives the estimates of the reorganization free energies λ_M computed from the parabolic fits according to (17) and (18) as well as the activation free energy using (32). These results are in excellent agreement with the predictions of the Marcus model ((41), (42) and (44)). However, even for Ag^{1+}/Ag^{2+}, despite of the asymmetries (Fig. 3) parabolic fit functions approximate the simulation data reasonably well. Deviations are largest in the equilibrium region of Ag^{+}.

We emphasize again that (28) used for the construction of the nonequilibrium parts of the curves is valid for every system, Gaussian or not. For Ag we have verified this relation, the most fundamental of gap laws, by comparing to the full diabatic free energy profiles computed using the FEP umbrella sampling method outlined in Sect. 2.3. Three intermediate windows were generated by selecting three values for the coupling parameter η in the bias potential of (23). The values we used were $\eta = 0.25$, 0.5, and 0.75 bridging the gap between the terminal $\eta = 0$ and $\eta = 1$ windows given by the equilibrium

results of Fig. 3. The results are reported in [33]. The FEP/US $A_M(\epsilon)$ profiles closely follow the parabolic fits in Fig. 5. The largest deviations are observed for gap values in the interval $\Delta E_\mu = 0.5 - 1$ eV. This is the region where most of the coordination number fluctuations are found to occur, confirming that they might be responsible for the non-linear behaviour [33].

The results for Ru^{2+}/Ru^{3+} and Ag^{1+}/Ag^{2+} confirm that the diabatic energy gap can be used as reaction coordinate for redox reactions, both in the Marcus regime and outside. Are there alternatives? The question is of interest because total energy gaps come with a number of technical complications for *ab initio* MD applications. One of the difficulties discussed in Sect. 3 is the computation of excited electronic states. Another drawback is that energy gaps prohibit the use of constraint methods. In this still rather popular method the free energy profiles are obtained as integrals over the mean force acting on the reaction coordinate (hence the name potential of mean force) [52]. The reaction coordinate is fixed at a series of values and the mean force is estimated from the force of constraint. So in the notation of Sect. 2.2

$$A(x) - A(x_0) = \int_{x_0}^{x} dx' \left\langle \frac{\partial H}{\partial X} \right\rangle_{X=x'} = -\int_{x_0}^{x} dx' \lambda_X(x') \tag{52}$$

where $\lambda_X(x')$ is the time average of the Lagrange parameter keeping the value of $X\left(\mathbf{R}^N\right)$ fixed at x' during the MD run (the last identity is approximate, for the corrections see [52]). This approach in practice requires that the reaction coordinate is available as an explicit function of configuration. Total energy is an implicit function so cannot be subjected to mechanical constraints.

Constraint methods, if applicable, are easy to use in *ab initio* MD which motivated us to search for configurational reaction coordinates to describe the Ru^{2+}/Ru^{3+} and Ag^{1+}/Ag^{2+} half reactions, preferably a structural (geometric) parameter. The coordination change we observed for Ag^{1+}/Ag^{2+} suggests that coordination number (n_c) might be used for this purpose in this system, which is what we tried in the work reported in [29]. The PMF we obtained is reproduced in Fig. 6. The contrast with Fig. 5 is striking. While there is a maximum in the PMF around $n_c = 4.6$, its value is one order of magnitude smaller than the activation free energy at the curve crossing in Fig. 5 (see also Table 2). The apparent barrier in Fig. 6 of 17 mev (=195 K) is well in the thermal range, implying that spontaneous oxidation might occur on the MD time scale. The reason that these events are not observed is that n_c is evidently inadequate as a reaction coordinate (in fact as the analysis in [33] shows n_c is not even a good order parameter for distinguishing unambiguously between oxidation states). The transition dynamics is dominated by solvent rearrangements which are not represented by the PMF for n_c. The consequence is underestimation of the free energy of activation. This phenomenon is now well understood thanks of the work of the Chandler group (see for example [53, 54] and the chapter on transition path sampling in this book). The special point for us here is that the solvent reorganization is much better accounted for by the free energy of the diabatic energy gap. This feature

of diabatic energy gaps has been repeatedly emphasized by Warshel (see in particular [8, 10, 11]).

The discussion above raises the question whether perhaps the classical electrostatic point charge energy gap (11), while a (probably poor) approximation to the full electronic energy gap, could non the less play a similar role as reaction coordinate capturing the solvent reorganization. The idea would be to simply assign SPC charges to the H and O atoms of the solvent and compute the electrostatic potential at the site of the ion by standard Ewald methods. What is gained is that the mean force for this quantity can be determined using mechanical constraint methods or included among the metadynamics variables. The vertical SPC gap ΔU for half reactions is given directly by the electrostatic potential (10). The derivation is similar to the one given for the ET gap in Sect. 2. As we already have established that the $Ru^{+2} \rightarrow Ru^{3+} + e^-$ reaction adheres closely to the Marcus rules, this system seems a good candidate to subject this idea to a test. For the purpose of comparison to the fully consistent DFT results of Fig. 4 it is convenient to "calibrate" ΔU by the ionization energy in vacuum, denoted by ΔE_0^{v}, leading to the following expression for the classical vertical gap

$$\Delta U_\mu(\mathbf{R}^N) = \Phi(\mathbf{R}^N) + \frac{\xi_{\mathrm{EW}}}{2L}(q_{\mathrm{O}}^2 - q_{\mathrm{R}}^2) + \Delta E_0^{\mathrm{v}} + \mu \tag{53}$$

We have also included the self interaction energy of the ion with its periodic images and background charge in a finite periodic cell [55]. The Ewald constant $\xi_{\mathrm{EW}} = -2.837297$ and L is the box length. q_M is the classical point charge of the ion in state M. Finally, to be consistent with the bias applied to the quantum gap ΔE_μ (see (48)) we have also offset ΔU by an adjusted electronic chemical potential μ ensuring that reduced and oxidized state are strictly thermodynamically equivalent ($\Delta A_\mu = 0$).

The PMF for the SPC gap of Ru^{2+}/Ru^{3+} is compared to the full quantum gap free energy profile in Fig. 4. Only the lower energy (adiabatic) part has

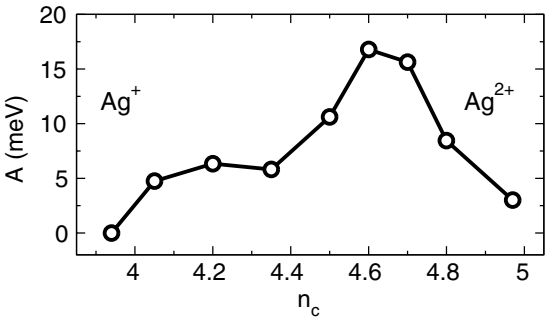

Fig. 6. Potential of mean force for the oxygen coordination number n_c of the Ag aqua cation. $n_c = 4$ for Ag^{1+} and $n_c = 5$ for Ag^{2+}. Oxidation takes place at $n_c = 4.6$ (data taken from [29]). Note the difference in energy scale with Fig. 5

been computed. It is clear, however, that the free energy profiles along the SPC gap are again harmonic but the curvature of the Ru^{3+} curve is almost twice larger than for Ru^{2+}. The same factor two difference is found for the variance of the equilibrium fluctuations (Table 2). In contrast to the quantum gap, the Marcus condition (38) is not satisfied for the classical gap. There is no conflict because (38) is only valid for the true energy gap of a Gaussian system. However, consistent with the larger width, also the activation free energy of $\Delta A_c^\dagger = 0.08$ eV predicted by the maximum in the PMF of the classical gap is lower than the estimate $\Delta A_q^\dagger = 0.20$ eV obtained for the quantum gap. Because the Ru cation is such a well behaved Marcus ion and ΔE_μ rather than ΔU_μ satisfies all the Marcus rules, we can be confident that $\Delta A_q^\dagger$ is the more reliable number. The classical electrostatic potential generated by fixed charges on the solvent atoms can be assumed to account for most of the reorganization of the orientational (inertial) solvent polarization. This can be concluded from all the work on classical models of aqueous Fe^{2+}/Fe^{3+} charge transfer, which showed that when ΔU is the consistent vertical gap the PMF is again symmetric. [7,12,14,16,21,22,24,25]. When the gap is only an approximation to the true total energy gap we can expect deviations from linear response. What is surprising, is that this effect for the Ru^{2+}/Ru^{3+} is as large as we found it to be.

4.3 Conclusion

The examples discussed in this section were meant to illustrate the use of the vertical diabatic energy gap as reaction coordinate for the study of redox reactions. First of all the energy gap proves to be an appropriate microscopic degree of freedom to represent the solvent polarization in Marcus theory. Because of its special status in free energy perturbation methods it also leads to a set of convenient and efficient expressions for the computation of the reaction free energy change of redox reactions. The most intriguing aspect of the energy gap is perhaps its potential for the computation of activation free energies. As the connection to Marcus theory already suggests, it seems to be a most suitable reaction coordinate to describe the for redox reactions all important solvent reorganization. Because of limitations in current DFT implementations, we focused on half reactions. The challenge is now to extend these methods to full electron transfer and redox reactions.

Acknowledgments

The following people have been collaborating with us in this ongoing project on redox reactions: Ivano Tavernelli, Yoshitaka Tateyama, Joost VandeVondele, Marialore Sulpizi, Regla Ayala Espinar and Rodolphe Vuilleumier. We thank them for their many and crucial contributions.

References

1. R. A. Marcus (1956) Theory of oxidation-reduction reactions involving electron transfer.1. *J. Chem. Phys.* **24**, p. 966
2. R. A. Marcus (1960) Theory of oxidation-reduction reactions involving electron transfer.4. A statistical-mechanical basis for treating contributions from solvent, ligands, and inert salt. *Discuss. Faraday Soc.* **29**, p. 21
3. R. A. Marcus (1965) On theory of electron-transfer reactions.6. Unified treatment for homogeneous and electrode reactions. *J. Chem. Phys.* **43**, p. 679
4. R. A. Marcus (1993) Electron-transfer reactions in chemistry – theory and experiment. *Rev. Mod. Phys.* **65**, p. 599
5. A. Warshel (1982) Dynamics of reactions in polar-solvents – semi-classical trajectory studies of electron-transfer and proton-transfer reactions. *J. Phys. Chem.* **86**, p. 2218
6. J. K. Hwang and A. Warshel (1987) Microscopic examination of free-energy relationships for electron-transfer in polar-solvents. *J. Am. Chem. Soc.* **109**, p. 715
7. G. King and A. Warshel (1990) Investigation of the free-energy functions for electron-transfer reactions. *J. Chem. Phys.* **93**, p. 8682
8. R. P. Muller and A. Warshel (1995) ab-initio calculations of free-energy barriers for chemical-reactions in solution. *J. Phys. Chem.* **99**, p. 17516
9. J. Bentzien, R. P. Muller, J. Florian, and A. Warshel (1998) Hybrid ab initio quantum mechanics molecular mechanics calculations of free energy surfaces for enzymatic reactions: The nucleophilic attack in subtilisin. *J. Phys. Chem. B* **102**, p. 2293
10. J. Villa and A. Warshel (2001) Energetics and dynamics of enzymatic reactions. *J. Phys. Chem. B* **105**, p. 7887
11. M. Strajbl, G. Hong, and A. Warshel (2002) Ab initio QM/MM simulation with proper sampling: "First principle" calculations of the free energy of the autodissociation of water in aqueous solution. *J. Phys. Chem. B* **106**, p. 13333
12. R. A. Kuharski, J. S. Bader, D. Chandler, M. Sprik, M. L. Klein, and R. W. Impey (1988) Molecular-model for aqueous ferrous ferric electron-transfer. *J. Chem. Phys.* **89**, p. 3248
13. E. A. Carter and J. T. Hynes (1989) Solute-dependent solvent force-constants for ion-pairs and neutral pairs in a polar-solvent. *J. Phys. Chem.* **93**, p. 2184
14. R. B. Yelle and Y. Ichiye (1997) Solvation free energy reaction curves for electron transfer in aqueous solution: Theory and simulation. *J. Phys. Chem. B* **101**, p. 4127
15. K. Ando (1997) Quantum energy gap law of outer-sphere electron transfer reactions: A molecular dynamics study on aqueous solution. *J. Chem. Phys.* **106**, p. 116
16. K. Ando (2001) Solvent nuclear quantum effects in electron transfer reactions. II. Molecular dynamics study on methanol solution. *J. Chem. Phys.* **114**, p. 9040
17. K. Ando (2001) Solvent nuclear quantum effects in electron transfer reactions. III. Metal ions in water. Solute size and ligand effects. *J. Chem. Phys.* **114**, p. 9470
18. K. Ando (2001) A stable fluctuating-charge polarizable model for molecular dynamics simulations: Application to aqueous electron transfers. *J. Chem. Phys.* **115**, p. 5228

19. D. W. Small, D. V. Matyushov, and G. A. Voth (2003) The theory of electron transfer reactions: What may be missing? *J. Am. Chem. Soc.* **125**, p. 7470
20. T. Ishida (2005) Polarizable solute in polarizable and flexible solvents: Simulation study of electron transfer reaction systems. *J. Phys. Chem. B* **109**, p. 18558
21. D. A. Rose and I. Benjamin (1994) Molecular-dynamics of adiabatic and nonadiabatic electron-transfer at the metal-water interface. *J. Chem. Phys.* **100**, p. 3545
22. D. A. Rose and I. Benjamin (1995) Solvent-free energies for electron-transfer at a solution metal interface – effect of ion charge and external electric-field. *Chem. Phys. Lett.* **234**, p. 209
23. J. B. Straus and G. A. Voth (1993) A computer-simulation study of free-energy curves in heterogeneous electron-transfer. *J. Phys. Chem.* **97**, p. 7388
24. J. B. Straus, A. Calhoun, and G. A. Voth (1995) Calculation of solvent-free energies for heterogeneous electron-transfer at the water-metal interface – classical versus quantum behavior. *J. Chem. Phys.* **102**, p. 529
25. A. Calhoun and G. A. Voth (1998) Isotope effects in electron transfer across the electrode-electrolyte interface: A measure of solvent mode quantization. *J. Phys. Chem. B* **102**, p. 8563
26. C. Hartnig and M. T. M. Koper (2001) Molecular dynamics simulations of solvent reorganization in electron-transfer reactions. *J. Chem. Phys.* **115**, p. 8540
27. C. Hartnig and T. M. Koper (2004) Molecular dynamics simulation of solvent reorganization in ion transfer reactions near a smooth and corrugated surface. *J. Phys. Chem. B* **108**, p. 3824
28. J. Blumberger, L. Bernasconi, I. Tavernelli, R. Vuilleumier, and M. Sprik (2004) Electronic structure and solvation of copper and silver ions: A theoretical picture of a model aqueous redox reaction. *J. Am. Chem. Soc.* **126**, p. 3928
29. J. Blumberger and M. Sprik (2004) Free energy of oxidation of metal aqua ions by an enforced change of coordination. *J. Phys. Chem. B* **108**(21), p. 6529
30. J. Blumberger and M. Sprik (2005) Ab initio molecular dynamics simulation of the aqueous Ru_{2+}/Ru_{3+} redox reaction: The Marcus perspective. *J. Phys. Chem. B* **109**, p. 6793
31. Y. Tateyama, J. Blumberger, M. Sprik, and I. Tavernelli (2005) Density-functional molecular-dynamics study of the redox reactions of two anionic, aqueous transition-metal complexes. *J. Chem. Phys.* **122**, p. 234505
32. J. Blumberger and M. Sprik (2006) Quantum versus classical electron transfer energy as reaction coordinate for the aqueous Ru_{2+}/Ru_{3+} redox reaction. *Theor. Chem. Acc.* **115**, p. 113
33. J. Blumberger, I. Tavernelli, M. L. Klein, and M. Sprik (2006) Diabatic free energy curves and coordination fluctuations for the aqueous Ag^{+}/Ag^{2+} redox couple: A biased Born-Oppenheimer molecular dynamics investigation. *J. Chem. Phys.* **124**, p. 064507
34. I. Tavernelli, R. Vuilleumier, and M. Sprik (2002) Ab initio molecular dynamics for molecules with variable numbers of electrons. *Phys. Rev. Lett.* **88**, p. 213002
35. J. VandeVondele, R. Lynden-Bell, E. J. Meijer, and M. Sprik (2006) Density functional theory study of tetrathiafulvalene and thianthrene in acetonitrile: Structure, dynamics, and redox properties. *J. Phys. Chem. B* **110**, p. 3614
36. J. VandeVondele, M. Sulpizi, and M. Sprik (2006) From solvent fluctuations to quantitative redox properties of quinones in methanol and acetonitrile. *Angew. Chem. Intl. Ed.* **45**, p. 1936

37. R. Car and M. Parrinello (1985) Unified approach for molecular-dynamics and density-functional theory. *Phys. Rev. Lett.* **55**, p. 2471
38. V. May and O. Kühn Eds. (2004) Charge and energy transfer dynamics in molecular systems. Wiley-VH: 2nd edition
39. M. Tachiya (1993) Generalization of the marcus equation for the electron-transfer rate. *J. Phys. Chem.* **97**, p. 5911
40. R. W. Zwanzig (1954) High-temperature equation of state by a perturbation method.1. Nonpolar gases. *J. Chem. Phys.* **22**, p. 1420
41. J. P. Valleau and G. M. Torrie (1977) In *Modern Theoretical Chemistry*, Berne; B. J. Ed., vol. 5 Plenum, New York
42. D. Frenkel and B. Smit Eds. (1996) *Understanding Molecular Simulation – From Algorithms to Applications.* Academic Press: San Diego
43. J. G. Kirkwood (1935) Statistical Mechanics of Fluid Mixtures. *J. Chem. Phys.* **3**, p. 300
44. M. Souaille and B. Roux (2001) Extension to the weighted histogram analysis method: combining umbrella sampling with free energy calculations. *Comp. Phys. Comm.* **135**, p. 40
45. M. Tachiya (1989) Relation between the electron-transfer rate and the free-energy change of reaction. *J. Phys. Chem.* **93**, p. 7050
46. A. J. Bard and L. R. Faulkner, Eds. (2001) *Electrochemical Methods.* John Wiley & Sons, 2nd ed.
47. CPMD Version 3.x, The CPMD consortium, `http://www.cpmd.org`, MPI für Festkörperforschung and the IBM Zurich Research Laboratory
48. N. Troullier and J. Martins (1991) Efficient pseudopotentials for plane-wave calculations. *Phys. Rev. B* **43**, p. 1993
49. J. VandeVondele, M. Krack, F. Mohamed, M. Parrinello, T. Chassaing, and J. Hutter (2005) QUICKSTEP: Fast and accurate density functional calculations using a mixed Gaussian and plane waves approach. *Comp. Phys. Comm.* **167**, p. 103
50. The CP2K developers group, http://cp2k.berlios.de/ (2005)
51. C. Hartwigsen, S. Goedecker, and J. Hutter (1998) Relativistic separable dual-space Gaussian pseudopotentials from H to Rn. *Phys. Rev. B* **58**, p. 3641
52. M. Sprik and G. Ciccotti (1998) Free energy from constrained molecular dynamics. *J. Chem. Phys.* **109**, p. 7737
53. P. L. Geissler, C. Dellago, and D. Chandler (1999) Chemical dynamics of the protonated water trimer analyzed by transition path sampling. *Phys. Chem. Chem. Phys.* **1**, p. 1317
54. P. L. Geissler, C. Dellago, and D. Chandler (1999) Kinetic pathways of ion pair dissociation in water. *J. Phys. Chem. B* **103**, p. 3706
55. G. Hummer, L. R. Pratt, and A. E. Garcia (1998) Molecular theories and simulation of ions and polar molecules in water. *J. Phys. Chem. A* **102**, p. 7885